Theoretical Analysis of the Detectivity in N-p and P-n GaSb/GaInAsSb Infrared Photodetectors

Yuan Tian, Baolin Zhang, *Member, IEEE*, Tianming Zhou, Hong Jiang, and Yixin Jin

***Abstract*—In this paper, the detectivity as well as the quantum efficiency and the zero-bias resistance-area product in N-p and P-n GaSb/$Ga_{0.8}In_{0.2}As_{0.19}Sb_{0.81}$ infrared detectors is analyzed, based on the incident wavelength and the parameters of GaSb and $Ga_{0.8}In_{0.2}As_{0.19}Sb_{0.81}$. The results show that the detectivity for the N-p structure is much higher than that for the P-n structure. In addition, the tunneling mechanism in both heterostructures strongly decreases the performance of $Ga_{0.8}In_{0.2}As_{0.19}Sb_{0.81}$/GaSb detectors. The optimum detectivity is obtained when the zero-bias resistance-area product is limited by the generation-recombination mechanism. Furthermore, the detectivity in the N-p heterostructure is saturated with a small thickness of p-$Ga_{0.8}In_{0.2}As_{0.19}Sb_{0.81}$ while the one in the P-n heterostructure is maximum with the thickness of n-$Ga_{0.8}In_{0.2}As_{0.19}Sb_{0.81}$ in the range of 2.5–3 μm.**

NOTATION

n	Electron concentration in n-side
W_n	Width in n-side depletion region
l_p	Hole diffusion length in n-side
D_p	Hole diffusion coefficient in n-side
S_p	Surface recombination velocity in n-side
r_n	Reflection on the n-side surface
α_n	Absorption coefficient on the n-side
μ_e	Electron mobility
X_e	Transmission coefficient for electrons
t	Width in GaSb
d	Width in GaInAsSb
σ	Trap capture cross section
N_f	Trap density
m^*	Effective mass
p	Hole concentration in p-side
W_p	Width in p-side depletion region
l_e	Electron diffusion length in p-side
D_e	Electron diffusion coefficient in p-side
S_e	Surface recombination velocity in p-side
r_p	Reflectivity on th p-side surface
α_p	Absorption coefficient on the p-side
μ_p	Hole mobility
X_h	Transmission coefficient for holes
K	Boltzmann's constant
T	Detector temperature
q	Electronic charge

Manuscript received March 25, 1999; revised August 10, 1999. This work was supported by the National Advanced Materials Committee of China. The review of this paper was arranged by Editor P. K. Bhattacharya.

The authors are with Changchun Institute of Physics, Chinese Academy of Sciences, Changchun 130021, China (e-mail: snmocvd@public.cc.jl.cn).

Publisher Item Identifier S 0018-9383(00)01943-2.

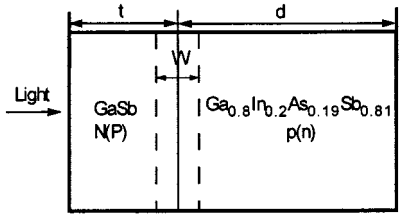

Fig. 1. Structure of GaInAsSb/GaSb detector.

A^*	$4\pi m^* qK^2/h^3$Effective Rechardson constant
δ	Fermi level

I. INTRODUCTION

QUATERNARY GaInAsSb alloys are of great interest for mid-infrared applications including infrared remote sensing systems, environmental monitoring and optical fiber communications [1]–[3]. They can be grown lattice-matched on GaSb substrates, and GaInAsSb/GaSb forms type-II heterojunctions with a staggered or broken alignment [4]. For the type-II band alignment, electrons and holes are separated at both sides of heteroboundary. Moreover the wide-band-gap material is considered as a window layer, in which the high-energy photons are absorbed in the wide-band gap material while the low-energy photons cross the wide-band-gap material and are absorbed in the narrow-band-gap material near the heterointerface. Alloys of GaInAsSb lattice-matched to GaSb span the wavelength range of 1.7–4.3 μm and thus the GaInAsSb/GaSb material system is ideally suited for devices to be used in this range. For example, Zhang [5] reported GaInAsSb/GaSb infrared photodetectors prepared by MOCVD for room-temperature operation at 2.25 μm. Shi [6] fabricated resonant cavity enhanced GaInAsSb photodectors grown by MBE for room-temperature operation at 2.35 μm. In this paper, the detectivity D^*, associated with the quantum efficiency η and the zero-bias resistance-area product R_0A, is calculated and analyzed for GaSb/$Ga_{0.8}In_{0.2}As_{0.81}Sb_{0.19}$ infrared photodetectors with N-p or P-n structures (upper-case letters present wide-band-gap materials and lower-case letters are narrow-band-gap materials).

II. THEORETICAL MODEL

The structure for a GaInAsSb/GaSb detector is shown in Fig. 1, in which the incident light is injected from the front surface of the GaSb material. Rich-GaSb GaInAsSb/GaSb

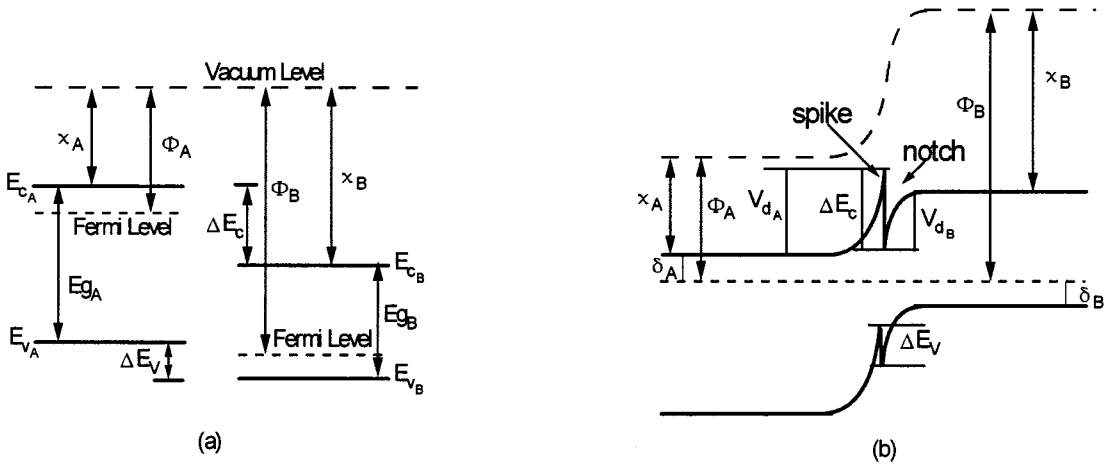

Fig. 2. Energy band profile before and after the formation of an abrupt N-p staggered type II heterojunction.

material systems are staggered type-II heterostructures. That is, either the conduction or the valence band of one semiconductor lies outside the bandgap of the other material, and the band offsets have the same sign (referring to the electron level), which is shown in Fig. 2(a). According to Anderson's model [7], when the two kinds of material form an abrupt p-n heterojunction, a spike and a notch occur in the conduction or valence band at the heterointerface. Fig. 2(b) shows the energy band profile of the staggered type-II N-p heterojunction. In order to get a clear definition of relevant physical quantities for the discontinuity of a heterojunction, the definition based on Fig. 2(b) is listed as follows[8].

1) Eg_A and Eg_B are the bandgaps of the wide- and narrow-band materials.
2) ΔEg is defined as the difference between the wide- and narrow-band semiconductors so that $\Delta Eg > 0$.
3) ΔE_c and ΔE_v are the conduction- and valence-band discontinuities at the heterointerface. $\Delta E_c > 0$ means that the conduction-band edge of the wide-band semiconductor is at a higher energy level compared to that of the narrow-band semiconductor, and vice versa if $\Delta E_c < 0$. $\Delta E_v > 0$ means that the valence-band edge of the wide-band semiconductor is at a lower energy level compared to that of the narrowband semiconductor, and vice versa if $\Delta E_v < 0$.
4) V_d is the built-in potential at the heterojunction depletion region and V_{dA}, V_{dB} are the barriers due to the band bending of the two sides of the heterointerface, respectively. $V_d > 0$ means that the band bending of the wide-band semiconductor is upward, and vice versa if $V_d < 0$.
5) δ is the distance between the Fermi-level and the band edge. For $\delta > 0$, the Fermi-level is in the forbidden band, while for $\delta < 0$, the Fermi-level is up above the conduction band or below the valence band.
6) X and Φ, defined as the electron affinity and work function of a given semiconductor, respectively, are energies required to remove an electron from the bottom of the conduction band (E_c) and from the Fermi-level (E_f) to the vacuum level, respectively.

Several simple equations linking the above quantities are listed:

$$V_d = V_{dA} + V_{dB} \tag{1}$$

$$\Delta E_c = X_A - X_B \tag{2}$$

$$\Delta Eg = Eg_A - Eg_B \tag{3}$$

$$\Delta E_c + \Delta E_v = \Delta Eg \tag{4}$$

$$\delta_A + \delta_B + V_d - \delta E_c = Eg_B \quad \text{(for an N-p heterostructure)} \tag{5}$$

$$\delta_A + \delta_B - V_d + \delta E_c = Eg_A \quad \text{(for a P-n heterostructure).} \tag{6}$$

In this paper, the selected structure is $Ga_{0.8}In_{0.2}As_{0.19}Sb_{0.81}$/GaSb, in which the lattice of $Ga_{0.8}In_{0.2}As_{0.19}Sb_{0.81}$ material is matched to GaSb. Thus, the effective wavelength range is in 1.7–2.5 μm. The figure of merit usually used to characterize the sensitivity of infrared photodetectors is the detectivity D^*, which depends on the wavelength of the incident light λ, the quantum efficiency η and the zero-bias resistance-area product R_0A,

$$D^* = \frac{q\eta\lambda}{hc}\sqrt{\frac{(R_0A)}{4KT}} \tag{7}$$

where $R_0A = KT/qJ_s$, and J_s is the saturated current.

As discussed in a homojunction GaInAsSb infrared detector [9], we consider four fundamental kinds of noise mechanisms in GaInAsSb/Gasb detectors: Auger and radiative mechanisms (both in the diffusion current) in the n and p neutral regions, generation-recombination mechanism (G-R) in the depletion region, and tunneling mechanism (corresponding to electrons and holes) through the barriers at the heterointerface. In this calculation, either for the N-p structure or for the P-n structure, the GaSb material is considered as a window layer, from the surface of which the light is incident, and only the photons with the energy lower than the GaSb bandgap can cross GaSb and reach GaInAsSb.

TABLE I
DIFFUSION AND TUNNELING CURRENTS AND THE ENERGY PROFILES IN THE HETEROSTRUCTURE.

	Energy band profile		p region	n region
N-p	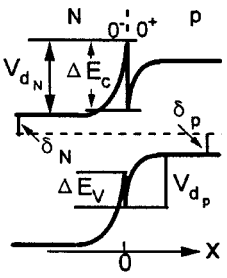	Diffusion current	$V_{d_p} > \Delta E_c$ $J_{s_n} = C_1 \exp\left[-q(V_d - \Delta E_c)/KT\right]$ $V_{d_p} < \Delta E_c$ $J_{s_n} = C_1 \exp\left[-qV_{d_N}/KT\right]$	$V_{d_N} > \Delta E_V$ $J_{s_p} = C_2 \exp\left[-q(V_d - \Delta E_v)/KT\right]$ $V_{d_N} < \Delta E_V$ $J_{s_p} = C_2 \exp\left[-qV_{d_p}/KT\right]$
		Tunneling current	$J_{s_p} = A^* T^2 P_p \exp\left(-\frac{V_{d_p} + \delta_p}{KT}\right)$ $E_{max}=\min[E_v(0^-), E_v(W_p)]$	$J_{s_N} = A^* T^2 P_N \exp\left(-\frac{V_{d_N} + \delta_N}{KT}\right)$ $E_{min}=\max[E_c(0^+), E_c(W_N)]$
P-n	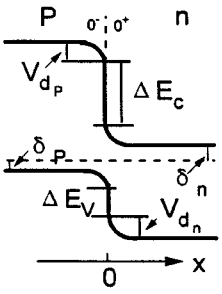	Diffusion current	$\Phi_P > \Phi_n$ $J_{s_n} = C_1 \exp\left[-q(V_d + \Delta E_c)/KT\right]$ $\Phi_P < \Phi_n$ $J_{s_n} = C_1 \exp\left[-q(\Delta E_c - V_{d_n})/KT\right]$	$\Phi_P > \Phi_n$ $J_{s_p} = C_2 \exp\left[-q(V_d + \Delta E_v)/KT\right]$ $\Phi_P < \Phi_n$ $J_{s_p} = C_2 \exp\left[-q(\Delta E_v - V_{d_P})/KT\right]$
		Tunneling current	$J_{s_P} = A^* T^2 P_P \exp\left(\frac{V_{d_P} - \delta_P + \Delta E_v}{KT}\right)$ $E_{max}=\min[E_v(0^-), E_v(W_N)]$	$J_{s_n} = A^* T^2 P_n \exp\left(\frac{V_{d_n} - \delta_n - \Delta E_c}{KT}\right)$ $E_{min}=\max[E_c(0^+), E_c(W_P)]$

A. Auger Mechanism and Radiative Mechanism

The diffusion current, the fundamental current in a p-n junction detector is determined by the Auger and radiative mechanisms [$(R_0A)_{\rm Auger}$ and $(R_0A)_{\rm Rad}$]. Because of the discontinuities in the bandedges at the heterointerface, the diffusion current in a p-n heterojunction is different from that in a p-n homojunction. Considered the transport of electrons in an N-p heterojunction in Fig. 2(b), only the electrons in the wide-band material with the energy higher than the barrier qV_{dA} can reach the heterointerface of the narrowband material, and similarly, the electrons in the narrowband material with the energy higher than the barrier $\Delta E_c - qV_{dB}$ can reach the heterointerface of the wideband material. These two components contribute to the electron diffusion current. The hole diffusion current has the same process. The diffusion currents for electrons and holes as well as the energy band profiles for N-p and P-n heterostructures are shown in Table I, respectively. In the diffusion currents, the parameters of C_1 and C_2 are given by

$$C_1 = qnX_e \frac{D_e}{L_e} \frac{\gamma_e \cosh\left(\frac{d-W_p}{L_e}\right) + \sinh\left(\frac{d-W_p}{L_e}\right)}{\gamma_e \sinh\left(\frac{d-W_p}{L_e}\right) + \cosh\left(\frac{d-W_p}{L_e}\right)} \tag{8}$$

$$C_2 = qpX_h \frac{D_h}{L_h} \frac{\gamma_h \cosh\left(\frac{t-W_n}{L_h}\right) + \sinh\left(\frac{t-W_n}{L_h}\right)}{\gamma_h \sinh\left(\frac{t-W_n}{L_h}\right) + \cosh\left(\frac{t-W_n}{L_h}\right)} \tag{9}$$

$$D = KT\mu/q, \quad L = (D\tau)^{1/2}, \quad \gamma = LS/D$$

where L is diffusion length.

B. Generation-Recombination Mechanism

As in an n-p homojunction, the carrier transport across a heterojunction is affected by the trap level in the depletion region, in which the current flow occurs by the generation-recombination of electron-hole pairs [10]. $(R_0A)_{\rm GR}$ is related with the intrinsic carrier concentration and the parameters in the depletion region [11], [12]. However, because of the discontinities in the heterojunction band edges at the heterointerface, the G-R mechanism is divided into two parts, $(R_0A)_{\rm GR}$ in the n and p depletion regions,

$$J_{s_{\rm GR_c}} = \frac{2KTn_{ic}w_c\sigma N_f}{V_{d_c}} \sqrt{\frac{3KT}{m_c^*}}. \tag{10}$$

The subscript c presents the material type.

C. Tunneling Mechanism

In type-II heterojunctions, both electrons and holes are separated at the both sides of the heteroboundary. If the thickness of the barrier is sufficiently thin, the electrons and holes with energy below the barrier can cross the heterointerface to form the tunnel current, which is an important noise mechanism [13], [14]. A numerical model for tunneling across the heterointerface is presented by developing a therminoic-field emission boundary condition, which is formulated based on the WKB approximation, and the detailed derivation is described in [13]. There, only the electron tunneling in the conduction band was considered. However, for the staggered type-II heterojunction, a barrier exists at the heterointerface of the valence band and the hole tunneling must be considered. The tunneling currents

in p and n regions for N-p and P-n heterostrucutures are also shown in Table I. In the tunneling currents, the tunneling factors of P_n and P_p are given by

$$P_n = \frac{\exp\left(\frac{E_c(0^-)}{KT}\right)}{KT} \int_{E_{\min}}^{E_c(0^-)} T(E_x) \exp\left(-\frac{E_x}{KT}\right) dEx \tag{11}$$

$$P_p = \frac{\exp\left(-\frac{E_v(0^+)}{KT}\right)}{KT} \int_{E_v(0^+)}^{E_{\max}} T(E_x) \exp\left(\frac{E_x}{KT}\right) dEx. \tag{12}$$

$T(E_x)$ is the tunneling probability [15]

$$T(E_x) = \left[-2 \int_{x2}^{x1} \sqrt{2m^* E_x}\, \frac{dx}{\hbar}\right] \tag{13}$$

where x_1 and x_2 are defined as the position of beginning and end for carrier tunneling.

D. Quantum Efficiency

When photo flux F_0 is incident on the surface of the wide-band gap material, the generation rate of electron-hole pairs as a function at distance x from the surface is [16]

$$G = \alpha(\lambda)(1 - r_A)\Phi \exp[-\alpha(\lambda)x]. \tag{14}$$

Under the condition of low injection and an abrupt junction in a one-dimensional (1-D) model, at wavelength λ where the absorption coefficient is α, the quantum efficiency of a detector, from the three regions $(\eta_n, \eta_p, \eta_{dr})$, two neutral regions and a depletion one, are as follows.

1) Quantum Efficiency for the N-p Heterostructure [7], [17], [18]: See (15) and (16), shown at the bottom of the page, and

$$\eta_{dr} = (1 - r_N)\left[e^{-\alpha_N(t - W_n)} - e^{-(\alpha_N t + \alpha_p W_p)}\right]. \tag{17}$$

The total quantum efficiency is given by

$$\eta = \eta_N + \eta_{dr} + \eta_p. \tag{18}$$

2) Quantum Efficiency for the P-n Heterostructure: The expressions of the quantum efficiency for the P-n heterostructure are the same as those for the N-p heterostructure, but the parameters in the N-p heterostructure should be exchanged to the corresponding ones in the P-n heterostructure, which are shown as follows: $N \to P; r_N \to r_P; L_h \to L_e; W_N \to W_P; \alpha_N \to \alpha_P; \gamma_h \to \gamma_e; p \to n; L_e \to L_h; W_p \to W_n; \alpha_p \to \alpha_n; \gamma_e \to \gamma_h$.The definitions for L_h, L_e, γ_e, γ_h are the same as those in the diffusion currents.

The parameters before arrow are the ones in the N-p structure and those after arrow are in the P-n structure.

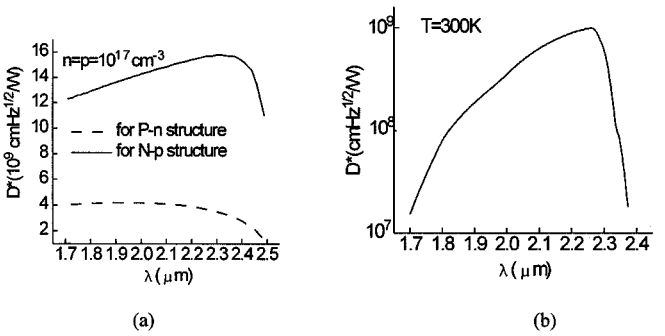

Fig. 3. Detectivity in N-p and P-n structures as a function of the incident photon wavelength with $n = p = 10^{17}$ cm^{-3}, $N_f = 10^{14}$ cm^{-3}, $\sigma = 10^{-15}$ cm^2 $S_e = S_p = 0$ and $t = 0.5$ μm, $d = 5$ μm (for the N-p structure) or $t = 5$ μm, $d = 0.5$ μm (for the P-n structure) and the experimental responsivity spectrum for p-$Ga_{0.8}In_{0.2}As_{0.18}Sb_{0.82}$/N-GaSb photodetector at zero bias with the incident light from the GaSb surface.

III. Results and Discussions

The calculations have been performed on p-N and n-P $Ga_{0.8}In_{0.2}As_{0.19}Sb_{0.81}$/GaSb infrared photodetectors at 300 K. The incident light is from the surface of the GaSb material with an ideal state, in which all photons with the energy lower than the bandgap of GaSb are assumed to cross GaSb and reach $Ga_{0.8}In_{0.2}As_{0.19}Sb_{0.81}$. Attenuation of the incident light due to the surface recombination, impurity absorption and lattice scattering, etc., is neglected. The dependence of GaInAsSb alloy parameters on the compositions x, y has been published in [19]. In our calculation, α and N_f in the p- and n depletion regions are assumed to be the same and the mobilities in the p and n regions are fixed to be $\mu_p = 240$ cm^2/V·s and $\mu_e = 10^3$ cm^2/V·s [20], respectively.

Fig. 3(a) shows the detectivity D^* in N-p and P-n structures as a function of the incident photon wavelength, with $n = p = 10^{17}$ cm^{-3}, $N_f = 10^{14}$ cm^{-3}, $\sigma = 10^{-15}$ cm^2 $S_e = S_p = 0$ and $t = 0.5$ μm, $d = 5$ μm (for the N-p

$$\eta_N = \frac{(1 - r_N)\alpha_N L_h}{\alpha_N^2 L_h^2 - 1} \times \left\{ \frac{\alpha_N L_h + \gamma_h - e^{-\alpha_N(t - W_N)}\left[\gamma_h \cosh\left(\frac{t - W_N}{L_h}\right) + \sinh\left(\frac{t - W_N}{L_h}\right)\right]}{\gamma_h \sinh\left(\frac{t - W_N}{L_h}\right) + \cosh\left(\frac{t - W_N}{L_h}\right)} - \alpha_N L_h e^{-\alpha_N(t - W_N)} \right\} \tag{15}$$

$$\eta_p = \frac{(1 - r_N)\alpha_N L_e}{\alpha_p^2 L_e^2 - 1} e^{-(\alpha_N t + \alpha_p W_p)} \times \left\{ \frac{(\gamma_e - \alpha_p L_e)e^{-\alpha_p(d - W_p)} - \left[\gamma_e \cosh\left(\frac{d - W_p}{L_e}\right) + \sinh\left(\frac{d - W_p}{L_e}\right)\right]}{\gamma_e \sinh\left(\frac{d - W_p}{Le}\right) + \cosh\left(\frac{d - W_p}{L_e}\right)} + \alpha_p L_e \right\} \tag{16}$$

structure) or $t = 5\ \mu$m, $d = 0.5\ \mu$m (for the P-n structure). Fig. 3(b) shows the experimental detecitivity D^* curve for p-$Ga_{0.8}In_{0.2}As_{0.18}Sb_{0.82}$/N-GaSb photodetector at zero bias with the incident light from the GaSb surface [5]. Fig. 3(a) clearly shows that D^* in the N-p heterostructure is much higher than that in the P-n heterostructure, which is caused by the quantum efficiency (η). In the N-p heterostructure, the quantum efficiency is mainly contributed by the component in p-$Ga_{0.8}In_{0.2}As_{0.19}Sb_{0.81}$, and the component in N-GaSb is zero in the ideal condition. The quantum efficiency in the P-n heterostructure is mainly contributed by the component in the n-$Ga_{0.8}In_{0.2}As_{0.19}Sb_{0.81}$ and the one in the P-GaSb is zero. The quantum efficiency we obtained is dependent on the minority-carrier diffusion current, in which the Auger and radiative mechanisms are included. At $p = n = 10^{17}\text{cm}^{-3}$, the minority-carrier diffusion length L_e and L_p in p- and n-$Ga_{0.8}In_{0.2}As_{0.19}Sb_{0.81}$ are $L_e = 218\ \mu$m and $L_p = 0.6\ \mu$m, respectively, which are determined by the temperature and minority-carrier lifetimes associated with Auger and radiative mechanisms. In p-$Ga_{0.8}In_{0.2}As_{0.19}Sb_{0.81}$, since $L_e \gg d$ (the p-side thickness) the most minority carriers, electrons, produced by the incident photons, will contribute to the diffusion current before recombineing. However, in n-$Ga_{0.8}In_{0.2}As_{0.19}Sb_{0.81}$, because of $L_p \sim d$ (the n-side thickness), only those minority carriers (holes) which do not recombine contribute to the diffusion current. Thus the quantum efficiency in p-$Ga_{0.8}In_{0.2}As_{0.19}Sb_{0.81}$ is higher than the one in the n-$Ga_{0.8}In_{0.2}As_{0.19}Sb_{0.81}$, which explains the higher D^* in the N-p heterostructure. In the N-p heterostructure, the maximum D^* is 1.58×10^{10} cmHz$^{1/2}$/W at $\lambda = 2.32\ \mu$m ($h\nu = 0.54$ eV) and the one in the P-n structure is 4.19×10^9 cmHz$^{1/2}$/W at $\lambda = 1.97\ \mu$m ($h\nu = 0.63$ eV). In Fig. 3(b), at the peak wavelength of 2.25 μm, the room temperature detectivity D^* is only 10^9 cmHz$^{1/2}$/W [5]. Comparing the calculated detectivity for the N-p heterostructure with the experimental one, the theoretical result is much higher than the experimental one. In the theoretical analysis, several hypotheses are considered, for example, the intensity of the incident photons does not decrease through GaSb; except for the four kinds of noise mechanisms; other kinds of noise mechanisms are neglected. However, in practice, all noise contribution should be taken into account in the detectors, which decreases the obtain the high detectivity. In addition, from the comparison between Fig. 3(a) and (b), we know that the detectivity of detectors will be increased with the improvement of the technology for the material growth and device fabrication.

As shown in Section II, $D^* \propto \eta\sqrt{R_0A}$. Therefore, it is necessary to analyze how the material parameters affect R_0A and η in order to obtain the optimum D^*. In the following, the influence of the material parameters on D^* as well as R_0A and η in the N-p and P—n heterostructures is discussed, with the wavelength of the incident light at the value where the maximum D^* is obtained. Because the energy of the incident light is lower than the GaSb bandgap, the quantum efficiency in GaSb is equal to zero in the ideal condition. In addition, only the carrier concentration in GaSb influences η by changing the thickness of the depletion region in $Ga_{0.8}In_{0.2}As_{0.19}Sb_{0.81}$. Other parameters, such as the thickness and surface recombination velocity of GaSb, will not change η. Moreover, because the diffusion current due to the minority carriers in GaSb is too small to affect R_0A, D^* is almost not influenced by the thickness and surface recombination velocity of GaSb, although both of them affect R_0A through Auger and radiative mechanisms. Therefore, our discussion is focused on the influence of the GaSb carrier concentration and the parameters of $Ga_{0.8}In_{0.2}As_{0.19}Sb_{0.81}$ on R_0A, η and D^*.

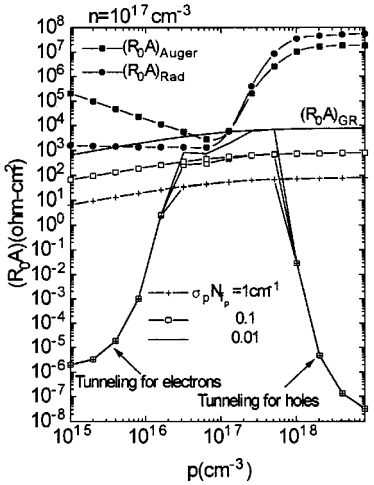

Fig. 4. The dependence of R_0A and its components on the carrier concentration of p-$Ga_{0.8}In_{0.2}As_{0.19}Sb_{0.81}$ (p) with $n = 10^{17}$ cm^{-3}, $\sigma N_f = 0.1$ cm^{-1}, $t = 0.5\ \mu$m, $d = 5\mu$ m and $S_e = S_p = 0$ in the N-p structure.

A. Detectivity in the N-p GaSb/$Ga_{0.8}In_{0.2}As_{0.19}Sb_{0.81}$ Heterostructure

Fig. 4 shows R_0A and its components as a function of the p-$Ga_{0.8}In_{0.2}As_{0.19}Sb_{0.81}$ carrier concentration (p), with $n = 10^{17}$ cm^{-3}, $t = 0.5\ \mu$m, $d = 5\ \mu$m and $S_e = S_p = 0$. In addition, R_0A and $(R_0A)_{\text{GR}}$ as a function of N_f and σ are also shown in Fig. 4. Because of $R_0A \propto (1/\sigma N_f)$, we just show the σN_f product as a parameter. From Fig. 4, we can see the following.

1) $(R_0A)_{\text{Auger}}$ and $(R_0A)_{\text{Rad}}$ are higher than those in n-p homostructure $Ga_{0.8}In_{0.2}As_{0.19}Sb_{0.81}$ detectors [9]. This is because that the barriers appear at the N-p heterointerface, not only for the conduction band but also for the valence band, which impede the minority-carrier diffusion. Therefore the diffusion current is reduced and the influence of the Auger and radiative mechanisms is weakened.
2) R_0A is limited by $(R_0A)_{\text{GR}}$ and $(R_0A)_{\text{Tunnel}}$, while $(R_0A)_{\text{Auger}}$ and $(R_0A)_{\text{Rad}}$ almost do not affect R_0A at $\sigma N_f = 0.1$ cm^{-1} or higher values. Because of $R_0A \propto (1/\sigma)N_f$, it is aninevitable outcome that if both N_f and σ is reduced, R_0A and D^* will be improved.
3) $(R_0A)_{\text{Tunnel}}$ is divided into two parts; the one for low p is caused by the electron tunneling in N-GaSb while the one for high p is by the hole tunneling in p-$Ga_{0.8}In_{0.2}As_{0.19}Sb_{0.81}$.
4) R_0A is dominated by the tunneling mechanism in the most range of p, and the tunneling mechanism strongly affects the performance of photodetectors. Only in the range

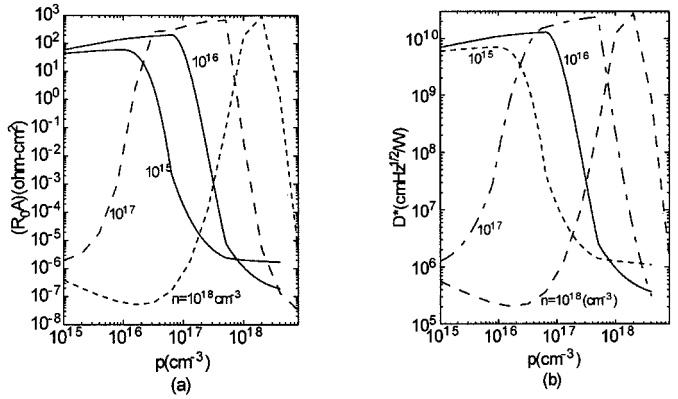

Fig. 5. Dependence of R_0A and D^* on the carrier concentration of p-$Ga_{0.8}In_{0.2}As_{0.19}Sb_{0.81}$ (p) with the carrier concentration of N-GaSb (n) as a parameter, in the condition of $\sigma N_f = 0.1$ cm^{-1}, $t = 0.5$ μm, $d = 5$ μm and $S_e = S_p = 0$ in the N-p structure.

of 3×10^{16} cm$^{-3} < p < 5 \times 10^{17}$ cm^{-3}, R_0A is limited by $(R_0A)_{\rm GR}$ and its optimum value can be obtained.

Fig. 5 shows R_0A and D^* as a function of the p-$Ga_{0.8}In_{0.2}As_{0.19}Sb_{0.81}$ carrier concentration (p) for several N-GaSb carrier concentrations (n), with $\sigma N_f = 0.1$ cm^{-1}, $t = 0.5$ μm, $d = 5$ μm and $S_e = S_p = 0$. D^* and its shape are controlled by R_0A. The tunneling mechanism strongly depends on the carrier concentration either in the N region or in the p region. In Fig. 5(a), $(R_0A)_{\rm GR}$ shows a little improvement at higher n and p. But, with increasing n, the electron tunneling increases, and at $n = 10^{18}$ cm^{-3}, becomes the main contribution to R_0A in the most range of low p. In contrast, the contribution of the hole tunneling to R_0A gradually decreases and becomes dominant at higher p. This is because, with increasing p and decreasing n, the built-in field and thickness of the N-GaSb depletion region become larger, both of which reduce the tunneling probability for electrons. On the contrary, the two factors increase the tunneling probability for holes. Except for the range where R_0A is controlled by the hole and electron tunneling, R_0A is limited by the G-R mechanism, and only in this range, the optimum D^* can be obtained. Additionally, in this range, although the maximum value of D^* is at $n = 10^{18}$ cm^{-3}, which is a little higher than those at $n = 10^{17}$ cm^{-3} or lower n, the range for the optimum D^* is much narrower than the others, which is disadvantageous in practice. In the material fabrication, if the N-GaSb carrier concentration is selected to be $n = 10^{18}$ cm^{-3}, the p-$Ga_{0.8}In_{0.2}As_{0.19}Sb_{0.81}$ carrier concentration must be controlled in a very narrow range to obtain the high D^*. Otherwise, the performance of detectors markedly declines because of the tunneling. However, if the carrier concentration in N-GaSb is selected as $n < 1018$ cm^{-3}, the carrier concentrations of the N- and p-side have a wide range to be chosen for optimum detector performance. In addition, for the material growth, it is easy to control the carrier concentration below to 10^{18} cm^{-3}.

Fig. 6 shows the dependence of R_0A, η and D^* on the p-$Ga_{0.8}In_{0.2}As_{0.19}Sb_{0.81}$ carrier concentration with the p-$Ga_{0.8}In_{0.2}As_{0.19}Sb_{0.81}$ surface recombination velocity (S_e) as a parameter, in the condition of $n = 10^{17}$ cm^{-3}, $\sigma N_f = 0.1$ cm^{-1}, $t = 0.5$ μm, $d = 5$ μm and $S_p = 0$. Because the change

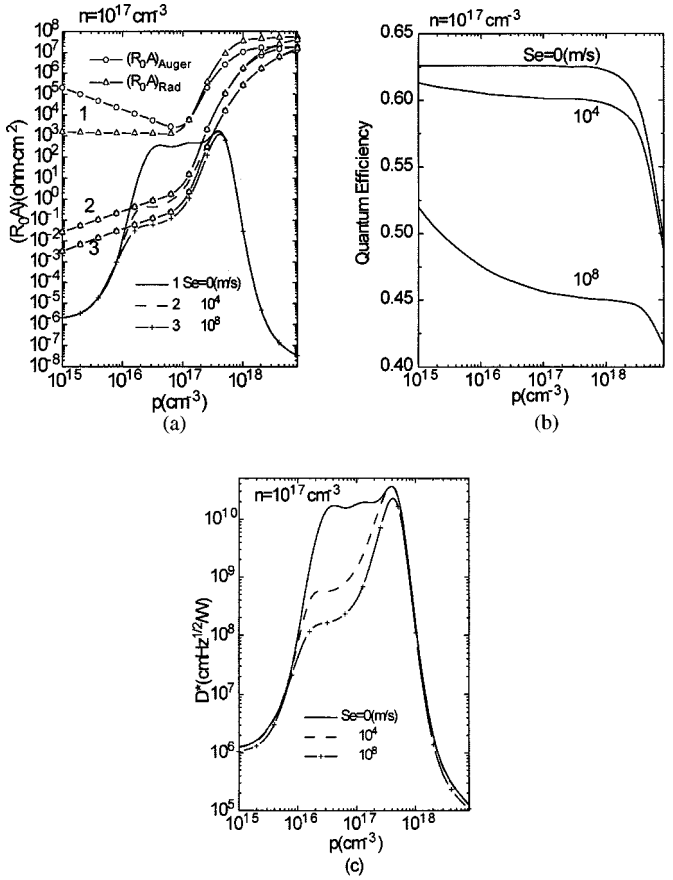

Fig. 6. Dependence of R_0A, η and D^* on the carrier concentration of p-$Ga_{0.8}In_{0.2}As_{0.19}Sb_{0.81}$ (p) with the surface recombination velocity of p-$Ga_{0.8}In_{0.2}As_{0.19}Sb_{0.81}$ (S_e) as a parameter, in the condition of $n = 10^{17}$ cm^{-3}, $\sigma N_f = 0.1$ cm^{-1} $t = 0.5$ μm, $d = 5$ μm and $S_p = 0$ in the N-p structure.

of S_e is associated with Auger and radiative mechanisms, $(R_0A)_{\rm Auger}$ and $(R_0A)_{\rm Rad}$ are also plotted in Fig. 6(a). Compared to the three parts of Fig. 6, it can be found that D^* is limited by R_0A and its shape is similar to that of R_0A, furthermore the quantum efficiency affects D^*. In an n-p homojunction $Ga_{0.8}In_{0.2}As_{0.19}Sb_{0.81}$ detector [9], the high p-side surface recombination velocity strongly reduces R_0A and η, and therefore D^* decreases. An effective way to reduce the surface recombination velocity is to grow an epitaxial layer on the p-$Ga_{0.8}In_{0.2}As_{0.19}Sb_{0.81}$ and to form homo- or heterointerface. We have reported that, in the n^+-n and p^+-p homojunctions, the heterointerface recombination velocities are effectively reduced [21].

R_0A is almost not affected by the p-$Ga_{0.8}In_{0.2}As_{0.19}Sb_{0.81}$ thickness (d) because R_0A is controlled by $(R_0A)_{\rm GR}$ in $p < 10^{18}$ cm^{-3}. However, η markedly increases with large d in this range because, since $L_e \gg d$, thicker thickness will improve the absorption for phonons. With d as a parameter, the dependence of η and D^* on p is similar to that in Fig. 6. Although the shape of D^* is similar to R_0A, the increase in η improves D^*. In order to find the maximum D^* and η with d, Fig. 7 shows η and D^* as a function of d with the same other parameters in Fig. 6 and $p = 5 \times 10^{17}$ cm^{-3} at which the optimum D^* is obtained. Because R_0A almost keeps as a constant with the change of d, η controls D^*. With the change of d, both η and D^* rapidly

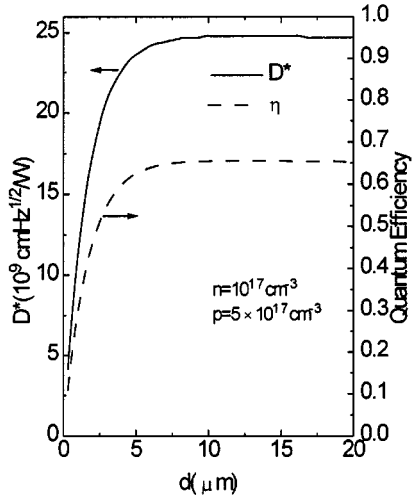

Fig. 7. Dependence of η and D^* on the thickness of p-$Ga_{0.8}In_{0.2}As_{0.19}Sb_{0.81}$ (d) with $n = 10^{17}$ cm^{-3}, $\sigma N_f = 0.1$ cm^{-1}, $t = 0.5$ μm, $d = 5$ μm, $S_e = S_p = 0$ and $p = 5 \times 10^{17}$ cm^{-3} in the N-p structure.

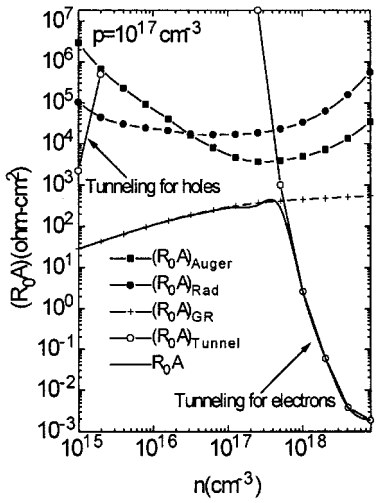

Fig. 8. Dependence of R_0A and its components on the carrier concentration of n-$Ga_{0.8}In_{0.2}As_{0.19}Sb_{0.81}$ (n) with $p = 10^{17}$ cm^{-3}, $\sigma N_f = 0.1$ cm^{-1}, $t = 5$ μm, $d = 0.5$ μm and $S_e = S_p = 0$ in the P-n structure.

increase and then saturate at $d > 10$ μm. The maximum η and D^* are 0.655 and 2.48×10^{10} cmHz$^{1/2}$/W, respectively.

B. Detectivity in the P-n GaSb/$Ga_{0.8}In_{0.2}As_{0.19}Sb_{0.81}$ Heterostructure

Fig. 8 shows R_0A and its components as a function of the n-$Ga_{0.8}In_{0.2}As_{0.19}Sb_{0.81}$ carrier concentration (n), with $p = 10^{17}$ cm^{-3}, $\sigma N_f = 0.1$ cm^{-1}, $t = 5$ μm, $d = 0.5$ μm, and $S_p = S_e = 0$. As in the N-p heterostructure, R_0A is limited only by $(R_0A)_{\rm GR}$ and $(R_0A)_{\rm Tunnel}$, while Auger and radiative mechanisms almost do not influence R_0A. $(R_0A)_{\rm Tunnel}$ is still divided into two parts: one is for holes and the other for electrons shown in Fig. 8. However, the tunneling current for holes is too low to contribute to R_0A. Therefore, in the range of $n < 10^{18}$ cm^{-3}, R_0A is limited by $(R_0A)_{\rm GR}$, and in the range of $n > 10^{18}$ cm^{-3} by $(R_0A)_{\rm Tunnel}$ (for electrons). It is clear that the low N_f and small σ will improve R_0A and D^*.

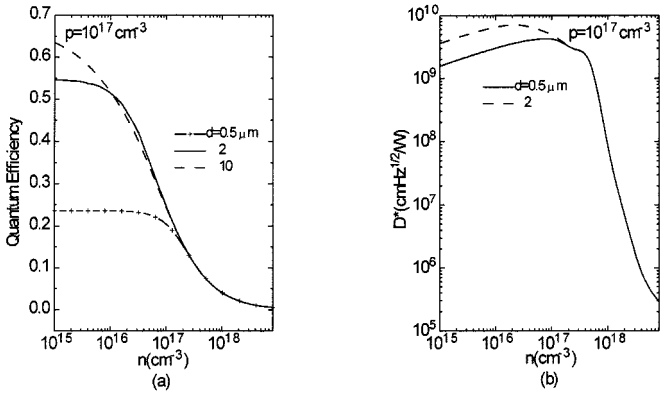

Fig. 9. Dependence of η and D^* on the n-side carrier concentration (n) with the thickness of n-$Ga_{0.8}In_{0.2}As_{0.19}Sb_{0.81}$ (d) as a parameter, in the condition of $p = 10^{17}$ cm^{-3}, $\sigma N_f = 0.1$ cm^{-1}, $t = 5$ μm, and $S_e = S_p = 0$ in the P-n structure.

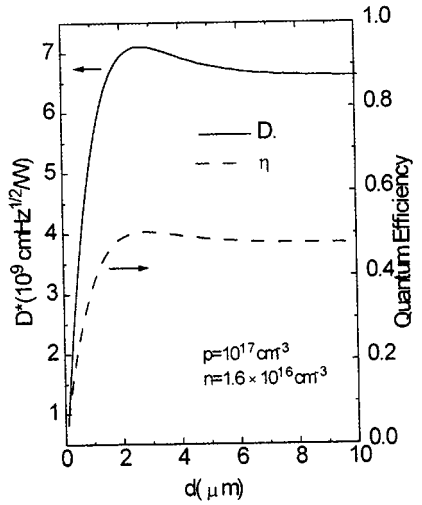

Fig. 10. Dependence of η and D^* as a function of the thickness of n-$Ga_{0.8}In_{0.2}As_{0.19}Sb_{0.81}$ (d) with $p = 10^{17}$ cm^{-3}, $\sigma N_f = 0.1$ cm^{-1}, $t = 5$ μm, $S_e = S_p = 0$, and $n = 1.6 \times 10^{16}$ cm^{-3} in the P-n heterostructure.

The dependence of η and D^* on n-$Ga_{0.8}In_{0.2}As_{0.19}Sb_{0.81}$ carrier concentration (n) is shown in Fig. 9 with the n-$Ga_{0.8}In_{0.2}As_{0.19}Sb_{0.81}$ thickness (d) as a parameter, with $p = 10^{17}$ cm^{-3}, $\sigma N_f = 0.1$ cm^{-1}, $t = 5$ μm, and $S_p = S_e = 0$. Although the large d reduces $(R_0A)_{\rm Auger}$ and $(R_0A)_{\rm Rad}$ in the n-$Ga_{0.8}In_{0.2}As_{0.19}$, R_0A is controlled by $(R_0A)_{\rm GR}$ in $n < 10^{18}$ cm^{-3} shown in Fig. 8 and the change of R_0A with d is very small compared to the influence of $(R_0A)_{\rm GR}$ and $(R_0A)_{\rm Tunnel}$. Therefore, R_0A is not shown in Fig. 9. The shape of D^* is similar to R_0A but the value of D^* is affected by η in $n < 10^{18}$ cm^{-3}. In addition, the large d will improve η and D^*, and the peak of D^* moves to the low n. In order to find the largest d for the optimum η and D^*, the dependence of η and D^* on d is plotted in Fig. 10 with the same value for other parameters as in Fig. 9 and $n = 1.6 \times 10^{16}$ cm^{-3} at which the maximum value of D^* is obtained. Unlike in Fig. 7, η and D^* increase quickly and go through a peak and at last saturate as d increases. The peak values of η and D^* are 0.504 and 7.1×10^9 cmHz$^{1/2}$/W, respectively, in the range of 2.5 μm$\leq d \leq 3$ μm.

As shown in Fig. 8, the optimum R_0A and D^* are controlled by the G-R mechanism. Moreover, with increasing the P-GaSb carrier concentration, $(R_0A)_{\rm GR}$ has a little improvement and therefore D^* increases a little, which is similar to that in Fig. 5.

IV. Conclusion

In this paper, the theoretical analysis of the detectivity associated with the quantum efficiency and the zero-bias resistance-area product is performed for N-p and P-n GaSb/$Ga_{0.8}In_{0.2}As_{0.19}Sb_{0.81}$ infrared photodetectors operated at 300 K, as a function of the wavelength of the incident light using the parameters of GaSb and $Ga_{0.8}In_{0.2}As_{0.19}Sb_{0.81}$. The calculated results show that the behavior of D^* depends on R_0A and η. The conclusions are as follows.

1) The detectivity for the N-GaSb/p-$Ga_{0.8}In_{0.2}As_{0.19}Sb_{0.81}$ detector is higher than that for the P-GaSb/n-$Ga_{0.8}In_{0.2}As_{0.19}Sb_{0.81}$ detector because the quantum efficiency in the p-$Ga_{0.8}In_{0.2}As_{0.19}Sb_{0.81}$ is higher than that in n-$Ga_{0.8}In_{0.2}As_{0.19}Sb_{0.81}$, which is a factor to determine D^*.
2) In both N-p and P-n structures, R_0A is limited by the generation-recombination and tunneling mechanisms. The tunneling mechanism strongly reduces R_0A and D^*. In the range where R_0A is controlled by $(R_0A)_{\rm GR}$, the optimum D^* can be obtained.
3) $(R_0A)_{\rm GR}$ is affected by the material carrier concentration, the trap density, and the trap capture cross section. The last two factors strongly change R_0A and D^*. The low N_f and σ effectively improve D^*. For example, with the same parameters in Fig. 4 for the N-p structure, at $\sigma N_f = 0.1$ cm^{-1}, D^* is about 2×10^{10} cmHz$^{1/2}$/W, while at $\sigma N_f = 0.01$ cm^{-1}, D^* can reach about 7×10^{10} cmHz$^{1/2}$/W. With increasing carrier concentration, either for the n-side or for the p-side, both R_0A and D^* have a little improvement.
4) With increasing surface recombination of the n- and p-$Ga_{0.8}In_{0.2}As_{0.19}Sb_{0.81}$, R_0A, η and D^* are reduced in the N-p and P-n structures. Additionally, R_0A is almost not affected by the thickness of $Ga_{0.8}In_{0.2}As_{0.19}Sb_{0.81}$. However, the influences of the thickness of $Ga_{0.8}In_{0.2}As_{0.19}Sb_{0.81}$ on η and D^* are different for the N-p and P-n structures. In the N-p structure, η and D^* reach saturation with a finite thickness of p-$Ga_{0.8}In_{0.2}As_{0.19}Sb_{0.81}$, while the maximum values of η and D^* are obtained with the thickness of n-$Ga_{0.8}In_{0.2}As_{0.19}Sb_{0.81}$ in the range of 2.5–3 μm.
5) Except for the carrier concentration in GaSb, D^* is almost not influenced by the thickness and the surface recombination of GaSb, both of which are associated with Auger and radiative mechanisms to affect R_0A. On the other hand, the energy of the incident light is lower than the GaSb bandgap, which makes η in GaSb zero in the ideal condition. Thus, the parameters of the thickness and surface recombination velocity in GaSb do not influence η. The total influence of the two factors determines that the two parameters do not affect D^*.

References

[1] Y. P. Yakovlev, T. N. Danilova, A. N. Imenkov, and M. P. Mikhailova, "Suppression of Auger recombination in the diode laser based on type II InAsSb/InAsSbP and InAs/GaInAsSb heterostructure," *Proc. SPIE*, vol. 3001, pp. 356–363, 1997.

[2] Z. A. Shellenbarger *et al.*, "GaInAsSb and InAsSbP photodetectors for mid-infrared wavelengths," *Proc. SPIE*, vol. 2999, pp. 25–33, 1997.

[3] H. K. Choi, C. A. Wang, G. W. Turne, and M. J. Manfra, "High-performance GaInAsSb thermophotovoltaic devices with an AlGaAsSb window," *Appl. Phys. Lett.*, vol. 77, pp. 3758–3760, 1997.

[4] M. P. Mikhailov and A. N. Titkov, "Type II heterojunction in the GaInAsSb/GaSb system," *Semicond. Sci. Tech.*, vol. 9, pp. 1279–1295, 1994.

[5] B. Zhang *et al.*, "GaInAsSb infrared photodetectors prepared by MOCVD," *Electron. Lett.*, vol. 31, pp. 830–832, 1995.

[6] Y. Shi *et al.*, "Resonant cavity enhanced GaInAsSb photodetectors grown by MBE for room temperature operation at 2.35 μm," *Electron. Lett.*, vol. 32, pp. 2268–2269, 1996.

[7] B. L. Sharma and R. K. Purohit, "Theory of heterojunction," in *Semiconductor Heterojunction*, New York: Pergamon, 1974, ch. 1, p. 1.

[8] G. Margaritondo, "The problem of heterojunction band discontinuities," in *Heterojunction Band Discontinuities Physics and Device Applicatons*, F. Capasso and G. Margaritondo, Eds, New York: Elsevier , 1987, ch. 2, p. 59.

[9] Y. Tian *et al.*, "Analysis of the R_0A product and detectivity in a GaInAsSb infrared photovoltaic detector," *J. Phys. D.*, vol. 31, pp. 3291–3297, 1998.

[10] A. Sasak and P. N. Rosson, "Carrier transport processes in p-n junction layer with a distribution for trap level," *Solid-State Electron.*, vol. 34, pp. 959–967, 1991.

[11] D. L. Smith, "Recombination current in a p-n heterojunction diode," *Phys. Stat. Sol. (a)*, vol. 44, pp. 381–390, 1977.

[12] A. Rogalsik, "Analysis of the R_0A product in n^+-p $Hg_{1-x}Cd_xTe$ photodiodes," *Infrared Phys.*, vol. 28, pp. 139–153, 1988.

[13] R. Q. Yang, M. Sweeny, D. Day, and J. M. Xu, "Interband tunneling in heterostructure tunnel diodes," *IEEE Trans. Electron. Devices*, vol. 38, pp. 442–446, 1991.

[14] K. Yang, J. East, and G. Haddad, "Numerical modeling of abrupt heterojunction using a thermionic-fied emisson boundary condition," *Solid-State Electron.*, vol. 36, pp. 321–330, 1993.

[15] R. H. Rediker, S. Stopek, and J. H. R. Ward, "Interface-alloy epitaxial heterojunctions," *Solid-State Electron.*, vol. 7, p. 621, 1964.

[16] H. J. Hovel, "Carrier collection, spectral respones, and photocurrent," in *Semiconductors and Semimetals, Vol. 11*, R. K. Willardson and A. C. Beer, Eds, New York: Academic, 1975, ch. 2, p. 8.

[17] D. Rosenfeid and G. Bahir, "The quantum efficiency of HgCdTe photodiodes in relation to the direction of illumination and to their geometry," *J. Appl. Phys.*, vol. 72, pp. 3034–3040, 1992.

[18] A. Rogalski and J. Rutkowski, "Effect of structure on the quantum efficiency and R_0A product fo lead-tin chalcogenide photodiodes," *Infrared Phys.*, vol. 22, pp. 199–208, 1982.

[19] Y. Tian *et al.*, "Theoretical analysis of the Auger mechanism in a GaInAsSb infrared photovoltaic detector," *Opt. Eng.*, vol. 37, pp. 1754–1762, 1998.

[20] A. Z. Li, Q. J. Zhong, and L. Y. Zheng, "Molecular beam epitaxial growth characterization and performance of high-detectivity GaInAsSb/GaSb PIN detectors operating at 2.0 to 2.6 μm," *J. Crystal Growth*, vol. 150, pp. 1375–1378, 1995.

[21] Y. Tian *et al.*, "Numerical analysis of the detectivity in n^+-n-p and p^+-p-n GaInAsSb infrared detectors," *Solid-State Electron.*, vol. 43, pp. 1879–1891, 1999.

Yuan Tian was born in Fushun, China. She received the B.S. degree in physics in Jilin University, China, in 1994. Since then, she has been pursuing the M.S. and Ph.D. degrees for semiconductor photo-electronic materials and devices at the Changchun Institute of Physics, Chinese Academy of Sciences, Changchun.

Baolin Zhang (M'98) received the M.S. degree in semiconductor physics and devices from Jilin University, China, in 1989.

He is currently a Researcher at Changchun Institute of Physics, Chinese Academy of Sciences, Changchun. His current research interests include the growth and characterization of III-V compounds via metalorganic vapor phase (MOVPE) technique, luminescence from silicon, and opto-electronic devices based on silicon materials.

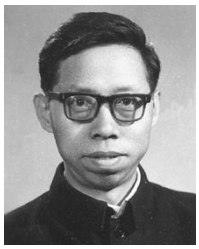

Tianming Zhou received the B.S. degree in physics from University of Science and Technology of China in 1964.

He has been a Researcher at Changchun Insitute of Physics, Chinese Academy of Sciences, Changchun, since 1964, and has worked on the growth of semiconductor materials and the research of optoelectronic devices. His current research interests include the growth and characterization of narrow bandgap III-V compounds and the infrared optoelectronic devices.

Hong Jiang received the B.S. degree from the Department of Electrical Science, Jilin University, Changchun, China, in 1986.

Since 1986, she has been with the Changchun Institute of Physics, where she has been working in the field of compound semiconductors, especially MOCVD growth of III-V compounds.

Yixin Jin received the B.S. degree from the Department of Physics, Peking University, Beijing, China, in 1965, and the degree of Docteur de L'Université en Sciences from the Université des Sciences et Techniques du Languedoc, France, in 1981.

Since 1965, he has been with Changchun Institute of Physics, Chinese Academy of Sciences, Changchun. From 1979 to 1981, he was with the Centre des Electroniques des Solides, Université des Sciences et Techniques du Languedoc. His interests cover luminescence materials and physics, preparation and characterization of opto-electronic materials, and functional materials. His current research interest is the materials in photonics.